



Characterising a Single-Photon Detector for ALPS II

Rikhav Shah¹ · Katharina-Sophie Isleif² · Friederike Januschek² · Axel Lindner² · Matthias Schott¹

Received: 30 October 2021 / Accepted: 28 March 2022 / Published online: 28 April 2022
© The Author(s) 2022

Abstract

Transition Edge Sensors (TESs) have found widespread application in fundamental studies due to their low background rate, high efficiency, and excellent energy resolution. This makes them suitable candidates for ALPS II, which investigates the existence of new particles (axions and axion-like-particles) which couple very weakly to photons. ALPS II anticipates an extremely low signal rate $< 10^{-5}$ cps (amounting to ~ 1 – 2 photons a day). The detection of these low energy (~ 1 eV, 1064 nm) photons with a high energy resolution is necessary for ALPS II. We show that with our TES setup, we can analyze the TES pulses with different methods such as pulse fitting and Principal Component Analysis (PCA). These achieve (using the standard deviation) an energy resolution ($\Delta E/E$) down to $\sim 8\%$. The pulse analysis, with a chosen fitting approach, assists also in achieving a very low dark count rate $\mathcal{O}(10^{-6})$ cps for 1064 nm photon signal searches in the TES.

Keywords TES · SQUID · Cryogenic single-photon detection · Pulse characterisation · Energy resolution · Backgrounds

1 Introduction

Transition Edge Sensors (TESs) have been shown to achieve low background rates and high detection efficiencies [1] for low-energy photon pulses. These salient features make TESs ideal candidates for use in the ALPS II experiment [2] at DESY, Hamburg, which uses a light-shining-through-a-wall implementation to search for new particles. These particles, namely axions and axion-like particles, exhibit very weak coupling to photons. Axions are a proposed solution to the strong *CP* problem in QCD [3–5] and, along with axion-like particles, can contribute to dark matter [6]. Their existence is also hinted at by astrophysical phenomena [7]. ALPS II strives to

✉ Rikhav Shah
rikhav.shah@desy.de

¹ Institute for Physics, Johannes Gutenberg-Universität Mainz, 55128 Mainz, Germany

² Deutsches Elektronen-Synchrotron DESY, Notkestr. 85, 22607 Hamburg, Germany

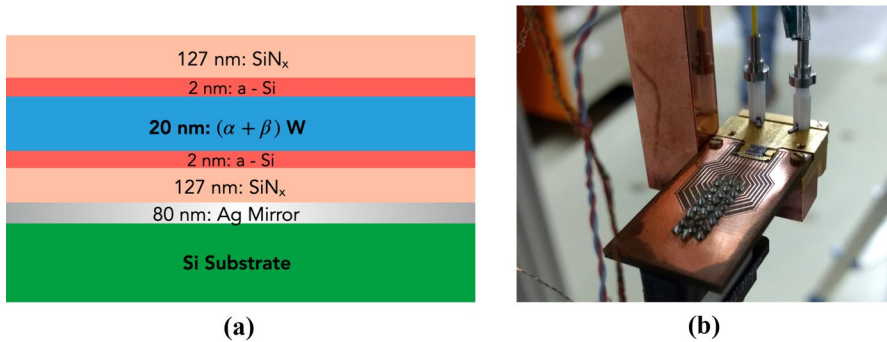


Fig. 1 (a) The cross-section of the TES ‘stack’ on the crystalline silicon substrate, with the 20 nm thick W TES, designed to achieve its T_C using the α, β phases of tungsten [11]. Figure adapted from Adriana Lita, private communication. (b) shows the TES detector module from PTB with the two fiber-coupled NIST TESs (inside white ferrules) and their bond wires to the SQUIDs, also integrated into the module by PTB. It is mounted on a copper finger. The approximate size of the module is: 1 cm \times 2 cm. (Color figure online)

achieve an axion-photon coupling sensitivity up to $g_{a\gamma\gamma} = 2 \times 10^{-11} \text{ GeV}^{-1}$. The rare conversion of axion-like-particles from and to photons (1064 nm photons are used in the cavity optics for ALPS II) in the presence of a magnetic field [8], leads to the extremely low signal rate $\sim 10^{-5}$ cps, at the aforementioned coupling. We calibrate the TES and analyze the low-energy (1.165 eV) 1064 nm pulses to achieve a good energy resolution and low background for ALPS II.

2 TES Detector Setup

TESs are cryogenic microcalorimeters operated in the region of their transition temperature, making use of the drastic change in their resistance in this region. In the ALPS II setup, the TES is a 20 nm thick tungsten film with dimensions $25 \mu\text{m} \cdot 25 \mu\text{m}$, from NIST (National Institute for Standards and Technology, USA). It has been optimised and designed for the detection of 1064 nm photons, using additional layers and anti-reflective coatings, as shown in the cross-sectional view in Fig. 1a. This ‘stack’ is deposited on a crystalline silicon substrate $\sim 375 \mu\text{m}$ thick. The detector module (shown in Fig. 1b) features two such TES chips. The chips are integrated into the module by the PTB (Physikalisch-Technische Bundesanstalt, Germany), along with dedicated SQUIDs (Superconducting Quantum Interference Devices) per chip to read out the sensors. These act as sensitive magnetometers and are operated and read out by dedicated electronics (XXF-1) from Magnicon GmbH, Hamburg. The entire setup is housed in a BlueFors dilution refrigerator (DR), capable of cooling down to a temperature < 25 mK. The critical temperature T_C of this TES is ~ 140 mK. A working point is chosen in the TES’s transition region by appropriately biasing the TES. This is realised in terms of (and corresponds to) a fraction of its normal conducting resistance $R_N \approx 10 \Omega$. The incidence and absorption of a single 1064 nm signal photon heats up the TES by $\sim 320 \mu\text{K}$, and, at a working point

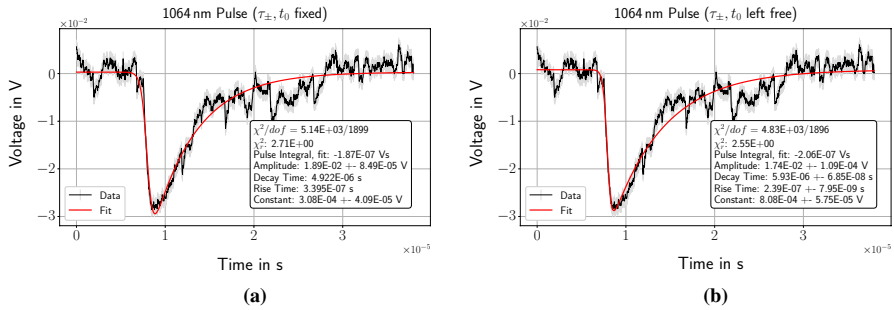


Fig. 2 An exemplary 1064 nm photon pulse is fitted with fixed time constants in (a); using $\tau_+ = 0.34 \mu\text{s}$ and $\tau_- = 4.92 \mu\text{s}$. These are average values from the ‘free’ fits (in (b)) of ~ 1000 1064 nm pulses. The same TES pulse is fitted in (b) without any time constant set to a fixed value. Minor differences from the ‘fixed’ approach can be seen in the fit itself, and the fit parameters. (Color figure online)

$0.3R_N$, leads to a macroscopic resistance change (following [9]). The corresponding pulses seen in the SQUID output (henceforth referred to as TES pulses) are analyzed to understand their critical parameters and pulse characteristics.

3 TES Pulse Characterisation and Energy Resolution

3.1 Pulse Fitting

1064 nm photons are introduced in the optical fiber-coupled TES using a strongly attenuated monochromatic continuous wave laser. The TES pulses consequently triggered in the data acquisition system¹ can be described with a function [10], following the small-signal limit. This function is not continuously differentiable with respect to time. To amend this and make the fitting more stable, the function is slightly modified to:

$$V_{out}(t) = C - \frac{2A}{\exp\left(-\frac{(t-t_0)}{\tau_+}\right) + \exp\left(\frac{(t-t_0)}{\tau_-}\right)}, \quad (1)$$

where τ_{\pm} are the rise and decay time constants of the pulse, A is its amplitude, t_0 is its trigger time (i.e. approximately the time of photon incidence), and C is a constant DC offset due to the setup and/or data acquisition. With τ_{\pm} and t_0 set to fixed values in the fitting procedure/minimizer, we obtain ‘pulse shape’ or ‘fixed’ fits (Fig. 2a), where the amplitude A and the offset C would be the only physical parameters varying.² Conversely, a ‘free fit’ on the pulse (Fig. 2b) is performed by leaving all

¹ The datasets generated during and/or analyzed during the current study is not publicly available due to ongoing analysis but are available from the corresponding author on reasonable request.

² With constant τ_{\pm} this would be proportional to the energy deposited in the TES.

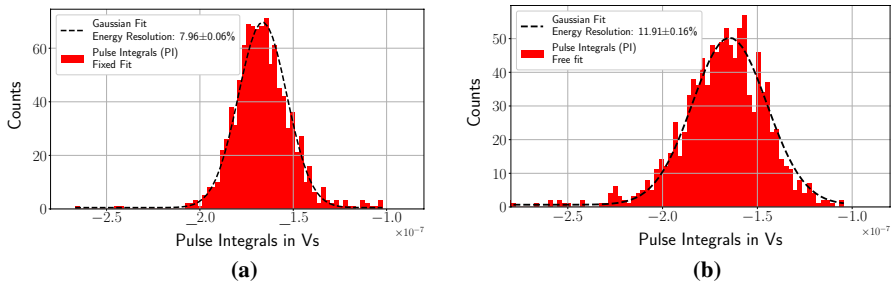


Fig. 3 (a) The distribution of the pulse integrals (as such, proportional to the energy deposited in the TES) for pulses fitted with fixed time constants, as in Fig. 2a. These are expressed in Volt seconds (Vs). An energy resolution of $(7.96 \pm 0.06)\%$ is achieved here, compared to the higher $(11.91 \pm 0.16)\%$ resolution in (b) for pulses with no parameter fixed (as in Fig. 2b). (Color figure online)

parameters free for fit optimisation. Average values from the ‘free’ fits of ~ 1000 1064 nm pulses are used to obtain $\tau_+ = 0.34 \pm 0.1 \mu\text{s}$ and $\tau_- = 4.92 \pm 0.7 \mu\text{s}$. A fixed fit could be performed using these values, for example, as shown in Fig. 2a. The ‘pulse shape’ approach is motivated by the TES response and feedback mechanism being identical for each pulse, where the TES returns to its equilibrium working point after photon absorption. This may not hold true for pulses with larger energy or influence of electrical noise, and each pulse would be described better individually using a ‘free fit’. Compared to the ‘pulse shape’ fits of single 1064 nm photons, photons of other wavelengths or pile-up events can have a substantially different shape and also different pulse height and/or χ^2 . These parameters can be used to distinguish them from 1064 nm photons. The pulse integrals (i.e. numerical integral of fitted data points over the pulse) are computed for the pulses from the fit performed. These are expected to scale with the energy deposited in the TES and are used to obtain the energy resolution; an example is shown in Fig. 3b. The pulse integral spectrum can be described as a Gaussian distribution, and we can calculate the resolution $ER = \Delta E/E = \frac{\sigma}{\mu}|_{\text{Gauss}}$, where μ is the mean of the distribution and σ is its standard deviation. A better energy resolution would mean higher distinguishing power for backgrounds, which is important for the ALPS II TES system. The operation of optical cavities in ALPS II, with the TES detector system, will use 532 nm light [12], which could also leak into the TES in small quantities and must be distinguished from the signal 1064 nm pulses. While ‘free’ fitted pulses have a worse ER of $(11.91 \pm 0.16)\%$ compared to the $(7.96 \pm 0.06)\%$ for ‘pulse shape’ fits, they capture more variation in the fit parameters. The electrical noise fluctuation in the TES setup is expected to be the primary cause of this variation.

3.2 Principal Component Analysis

As seen in the previous section, multiple variables can be used to characterise the TES response, which can be influenced by the electrical noise. This can hamper an efficient characterisation of the TES pulses. Using the well established Principal Component Analysis (PCA) approach to characterise the TES pulses, the

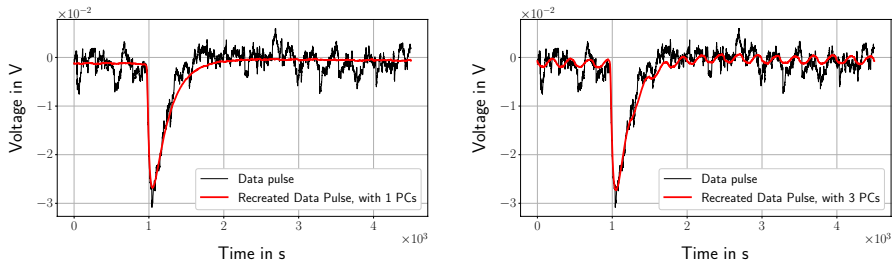


Fig. 4 The recreation of an exemplary 1064 nm photon pulse with principal components (PCs), which can reduce the influence of electrical noise. (Color figure online)

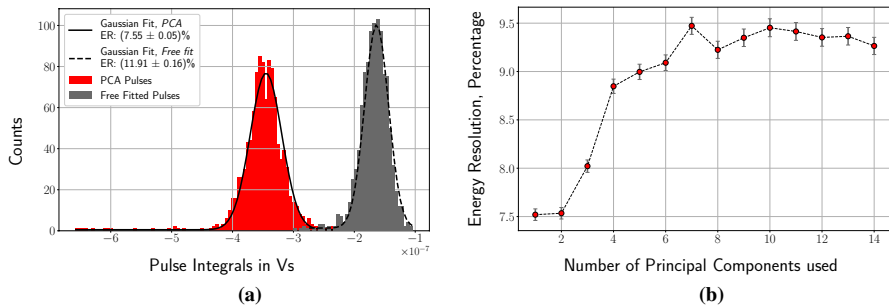


Fig. 5 (a) Compares the different energy resolutions of ~ 1000 1064 nm pulses, from free fits and with PCA recreation (using the first PC). The pulse integral calculated from the fitting procedure accounts for the DC offset C (seen in Fig. 2a, b), while the pulse integral calculated from the PCA (Fig. 4) does not, as the recreated pulses are not further analyzed with any fitting function. The pulse integral calculated with the PCA approach is consequently larger in magnitude. The use of PCs beyond the first two to recreate the pulse(s) worsens the energy resolution, as shown in (b). (Color figure online)

statistical variation and information of a dataset can be largely maintained while reducing its inherent dimensionality. For a single dataset, the data points in a pulse can be described as the weighted sum of ‘principal component (PC)’ basis functions (following [13, 14]). Each successive PC captures lesser and lesser information about the pulse(s). Using only the first few principal components to recreate the pulse can thus lead to a faithful reconstruction/recreation of the original pulses as seen in Fig. 4, where the use of only the first PC already traces the original TES pulse accurately.

Akin to the fitting procedure, the pulse integrals (numerical integral of the recreated pulse) can be used to obtain the energy resolution $\Delta E/E$, using a Gaussian function to fit the spectrum. This yields an energy resolution of $(7.55 \pm 0.05)\%$ recreated using only the first PC (Fig. 5a), for a dataset comprising of only (~ 1000) 1064 nm single-photon pulses. The use of further components beyond the second PC for pulse recreation worsens the energy resolution (Fig. 5b). Considering the ‘fixed’ fit method, the PCA approach results in a comparable energy resolution.

The PCA is not suitable for background rejection as it cannot reliably recreate the multiple kinds of pulses seen in a background-only dataset, due to the varying pulse shapes therein which can differ from each other, and 1064 nm signal photons quite strongly. The energy resolution is not of critical importance when it comes to background rejection, as other fit parameters (when using the free fit approach) assist in this procedure. This is not a feature of the PCA, which works best with a dataset of pulses with a single physical origin and shape, and provides just one principal component per analyzed pulse that can be reliably used for any pulse selection. The background analysis is thus better performed by the free fit procedure and is adopted as the baseline scheme for pulse discrimination.

3.3 Backgrounds

TES systems have low dark count rates, typically 10^{-2} cps or lower [15], which are negligible for signal rates $\mathcal{O}(100)$ Hz and higher. Comparatively, for our setup we need extremely low dark count rates, necessitating a deeper analysis of the backgrounds. In our system, we divide the backgrounds into two categories; the intrinsic backgrounds and the extrinsic backgrounds. The intrinsic backgrounds are pulses seen in the TES when there is no optical fiber connected to it (fiber-decoupled setup). The extrinsic backgrounds are the pulses seen in the TES with the optical fiber connected to it, but devoid of any optical signal input (dark fiber-coupled setup). The backgrounds could be comprised of radioactivity, cosmic rays, photons from black-body-radiation (expected to dominate the extrinsic backgrounds), electromagnetic fields, Cherenkov radiation, transition radiation (caused perhaps also by cosmic rays), etc. The fit parameters of these backgrounds may vary significantly from those of 1064 nm light pulses (with the free fit approach), allowing us to reject the majority of the background events.

For ALPS II to reach its design sensitivity, the TES system must be able to detect 50 1064 nm photons with 50% detection efficiency over a 20-day period to achieve 5σ significance.³ This requires the TES system to have a dark rate lesser than 7.7×10^{-6} cps over a 20-day period. We implement a pulse selection method (based on the free fit approach for characterisation, with an energy resolution $\sim 12\%$) for intrinsic background pulses collected over a period of 20 days. From $\sim 37,000$ background pulses collected⁴ we obtain a dark rate of $6.9^{+2.62}_{-1.47} \times 10^{-6}$ cps [15] for 1064 nm photons, amounting to 12 photons over 20 days. This selection procedure, when applied to a dataset containing only 1064 nm signal photon pulses, retains more than 90% of the pulses.

³ Jan Hendrik Pöld and Hartmut Grote, “ALPS II-Design Requirement document”, Document number v3, Internal Communication.

⁴ For a voltage trigger threshold -20 mV for the raw data.

4 Summary and Outlook

A TES system for single-photon detection has been set up, with pulses that can be characterised using fitting- or PCA-based approaches. The ‘fixed’ and ‘free’ fit methods result in an energy resolution $(7.96 \pm 0.06)\%$ and $(11.91 \pm 0.16)\%$ at 1.165 eV respectively, marginally bested by the PCA which achieves a resolution $(7.55 \pm 0.05)\%$. As the free fit method yields the widest scope for pulse characterisation and for ALPS II, it is adopted as the baseline scheme for background rejection and pulse characterisation. A pulse selection approach based on this has been shown to achieve a background rate of $6.9^{+2.62}_{-1.47} \times 10^{-6}$ cps considering the intrinsic backgrounds only, which would be a viable background level for ALPS II. Current studies being undertaken will measure the efficiency of the TES, the linearity of the TES response for photons of different energies and studies for the extrinsic backgrounds. The simulation of the electrical noise in the TES setup is also being studied and used to understand the TES pulses. This has also shown a strong dependence of the energy resolution on the electrical noise, and corroborates the results seen with the fitting. A GEANT4 and Monte Carlo simulation of the TES detector is being set up, which will contribute to a better understanding of our backgrounds.

Acknowledgements We want to thank NIST, USA, for the TES devices and PTB, Berlin, Germany, for the SQUID sensors, module and support. We would also like to thank Manuel Meyer and José Alejandro Rubiera Gimeno for their valuable input and help, as well as our other ALPS collaborators.

Funding Open Access funding enabled and organized by Projekt DEAL.

Open Access This article is licensed under a Creative Commons Attribution 4.0 International License, which permits use, sharing, adaptation, distribution and reproduction in any medium or format, as long as you give appropriate credit to the original author(s) and the source, provide a link to the Creative Commons licence, and indicate if changes were made. The images or other third party material in this article are included in the article’s Creative Commons licence, unless indicated otherwise in a credit line to the material. If material is not included in the article’s Creative Commons licence and your intended use is not permitted by statutory regulation or exceeds the permitted use, you will need to obtain permission directly from the copyright holder. To view a copy of this licence, visit <http://creativecommons.org/licenses/by/4.0/>.

References

1. A.E. Lita et al., Adv. Photon Count. Tech. IV **7681**, 71–80 (2000). <https://doi.org/10.1117/12.852221>
2. R. Bähre et al., J. Instrum., T0900 (2013). <https://doi.org/10.1088/1748-0221/8/09/t09001>
3. F. Wilczek, Phys. Rev. Lett. **40**(5), 279 (1978). <https://doi.org/10.1103/PhysRevLett.40.279>
4. S. Weinberg, Phys. Rev. Lett. **40**(4), 223 (1978). <https://doi.org/10.1103/PhysRevLett.40.223>
5. R.D. Peccei, H.R. Quinn, Phys. Rev. Lett. **38**(25), 1440 (1997). <https://doi.org/10.1103/PhysRevLett.38.1440>
6. A. Ringwald, Phys. Dark Univ. **1**(1), 116 (2012). <https://doi.org/10.1016/j.dark.2012.10.008>
7. I.G. Irastorza, J. Redondo, Prog. Part. Nucl. Phys. **102**, 89 (2018). <https://doi.org/10.1016/j.pnpnp.2018.05.003>
8. P. Sikivie, Phys. Rev. Lett. **51**(16), 1415 (1983). <https://doi.org/10.1103/PhysRevLett.51.1415>
9. J. Dreyling-Eschweiler et al., J. Mod. Opt. **62**(14), 1132 (2015). <https://doi.org/10.1080/09500340.2015.1021723>
10. K.D. Irwin, G.C. Hilton, Cryog. Part. Detect. 63–150 (2005). https://doi.org/10.1007/10933596_3
11. A.E. Lita et al., IEEE Trans. Appl. Supercond. **15**(2), 3528 (2005). <https://doi.org/10.1109/TASC.2005.849033>

12. J.H. Pöld, A. Spector, EPJ Tech. Instrum. **7**(1), 1 (2020). <https://doi.org/10.1140/epjti/s40485-020-0054-8>
13. M. Schmidt et al., J. Low Temp. Phys. **193**(5), 1243 (2018). <https://doi.org/10.1007/s10909-018-1932-1>
14. P.C. Humphreys, New J. Phys. **17**(10), 103044 (2015). <https://doi.org/10.1088/1367-2630/17/10/103044>
15. R. Shah et al., PoS, **EPS-HEP2021**, 801 (2022). <https://doi.org/10.22323/1.398.0801>

Publisher's Note Springer Nature remains neutral with regard to jurisdictional claims in published maps and institutional affiliations.